In-situ vertical load test of piled raft foundation and corresponding simulation using 3D finite element analysis

Haruki Numoto[i], Mitsuo Nakamura[ii], Xi Xiong[iii] and Tatsunori Matsumoto[iv]

i) Researcher, Technical Research Institute, HASEKO Corporation, 3-1-1, Tsurumaki, Tama-city, Tokyo, 206-0034, Japan.

ii) Director, Technical Research Institute, HASEKO Corporation, 3-1-1, Tsurumaki, Tama-city, Tokyo, 206-0034, Japan.

iii) Assistant Prof., Faculty of Geoscience and Civil Engineering, Kanazawa 920-1192, Japan.

iv) Professor Emeritus, Kanazawa University, Kanazawa 920-1192, Japan.

ABSTRACT

Piled raft foundation is a common foundation structure that reduces settlement of structures by adding piles to raft foundation. It is well known that the bearing capacity and settlement behaviors of a piled raft foundation are complicated. Numerous experiments and analyses have been conducted to clarify the load sharing between piles and rafts and the settlement behavior of piled raft foundations. However, there are not so many cases in which the actual behaviors, such as the load sharing between piles and raft and the settlement, have been confirmed by in-situ loading experiments. In this study, an in-situ vertical load test on a piled raft foundation model was conducted on a test site. In the test site, volcanic cohesive soil was found below the top fill layer of 1 m thick. The volcanic soil layer was underlain by tuffaceous clay, sandy silt and sand layers. The piled raft foundation model was composed of a square concrete raft of 1.5m × 1.5 m × 0.5 m supported by four steel pipe piles with an outer diameter of 101.6 mm and a length of 3.5 m. 3-dimensional finite element simulation was conducted to get deeper insight into the bearing mechanism of the piled raft foundation model.

Keywords: piled raft foundation, in-situ vertical load test, bearing capacity, vertical stiffness, 3D finite element analysis

1 INTRODUCTION

Piled raft foundation is a common foundation structure which reduces the settlement of a structure by adding piles to the raft foundation. However, it is known that the bearing capacity and settlement properties of piled rafts are complicated due to the pile-soil interaction. As for bearing capacity and settlement of piled rafts, settlement measurements have been made on actual structures (e.g., Tsuchiya et al., 2011; Suzuki and Hamamoto, 2014) in addition to many experimental and analytical studies (e.g., Yamashita et al., 2015). However, many points remain unclear owing to the lack of in-situ test data. Therefore, it is important to further accumulate in-situ loading test data of piled raft foundation. Moreover, corresponding simulations based on numerical analyses of the in-situ loading test seem to be effective to get a deeper insight into the bearing capacity and the settlement behaviors of piled raft foundation.

In this study, in-situ vertical load tests on piled raft foundation models were carried out, and the corresponding simulations using 3D-finite element analyses were conducted.

2 EXPERIMENT OUTLINE

2.1 Outline of foundation models

Table 1 shows the outline of foundation models, while Fig. 1 shows the shapes of foundation models and the layout of measuring instruments. In addition to the piled raft model, a raft alone model and a single pile model were prepared for comparison purposes. The square raft of the piled raft model and the square raft alone model were RC (Reinforced Concrete) structures of 1.5 m × 1.5 m in area and 0.5 m in height. The piles of the piled raft model and the single pile model were

close-ended steel pipe piles having a length L = 3.5 m below the ground level, an outer diameter D =-101.6 mm and a wall thickness t = 4.2 mm. The piles of the piled raft were embedded in the raft by 0.2 m. The number of piles for piled raft was 4, and the centre-to-centre (C/C) pile spacing s was 700 mm ($s/D \fallingdotseq 7$). The piles were jacked in the ground quasi-statically.

As for measurement items, vertical displacements were measured at 4 points, and the horizontal displacements in the x and y directions were measured at 2 points with strain gauge type displacement transducers. The earth pressures under the raft were measured at 3 points with load cell type soil pressure gauges. The same applies to the measurement items of the raft alone model. In addition, as shown in Fig. 1, strain gauges were installed at 8 different depths for pile A, pile D and the single-pile model, and at 5 different depths for pile B and pile C

Table 1. Outline of foundation models.

Item		Piled raft	Raft alone	Single pile
Raft	Raft size (m)	1.5×1.5 h = 0.5	1.5×1.5 h = 0.5	-
Pile	Dia. D (mm)	101.6	-	101.6
	Wall thickness t (mm)	4.2	-	4.2
	Number of piles	4	-	1
	C/C pile spacing s (mm)	700 ($s/D \fallingdotseq 7$)	-	-
	Length L (m)	3.5	-	3.5

N.B. C/C pile spacing: center-to-center pile spacing

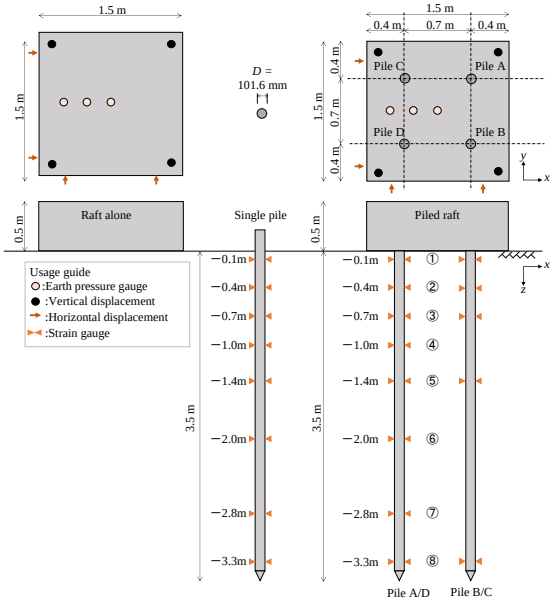

Fig. 1. Shapes of foundation models and arrangement of measuring instruments.

2.2 Ground conditions at the test site

Fig. 2 shows the profiles of soil layers and SPT N-values at the test site as well as the results of laboratory tests on soil. On the test site, volcanic cohesive soil was found below the top fill layer of 1 m thick. The volcanic soil layer was underlain by tuffaceous clay, sandy silt and sand layers. In the test, the backfilling soil layer was excavated down to the volcanic cohesive soil layer. The tip depth of the pile was GL-4.5 m, which was embedded in the sandy silt layer.

Unconfined compression tests of the soil specimens sampled at the site were conducted to obtain the unconfined compression strength q_u and secant modulus E_{50}. PS logging was carried out to obtain the shear wave velocity V_s and the corresponding shear modulus G ($G = \rho_t V_s^2$). Saturated unit weight γ_{sat} of soil was determined using the results of laboratory tests, which will be shown in Table 4 later. However, since the sand (GL -5.5 m or deeper) was not tested, it was assumed using the reference value in the unit weight of soil in the Recommendation for Design of Building Foundations (AIJ, 2019).

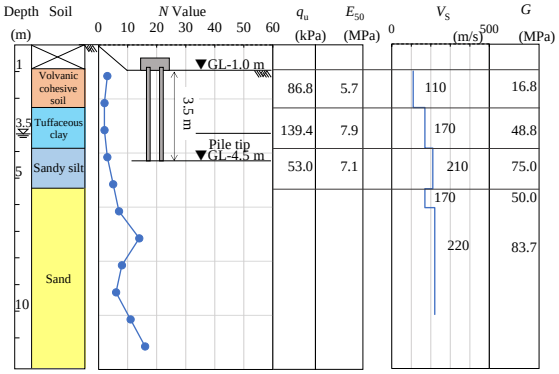

Fig. 2. Ground conditions at the test site.

2.3 Loading method

The loading method was a stepwise loading multi-cycle method according to the Japanese Geotechnical Society standards "Method for plate load test (JGS 1521-2012)" and "Method for static axial compressive load test of single piles (JGS 1811-2002)".

3 EXPERIMENTAL RESULTS

The total weight of the raft and the loading jig was 85 kN. Hence, loads carried by the raft and the piles prior to vertical loading are summarised in Table 2. Note that the load carried by the raft was estimated from the earth pressures at the raft base in the case of the piled raft. The load carried by the piles was estimated as 85 kN minus the raft load. The reason for that is foundation settlement due to the dead weight of the raft and the loading jig could not be measured.

Table 2. Initial load due to self-weight and jig-weight.

	Initial load (kN)	Load carried by raft (kN)	Load carried by 4 piles (kN)
Piled raft	85.0	21.0	64.0
Raft alone	85.0	85.0	-

3.1 Load-settlement relationship

Fig. 3 shows the relationship between the load P_V of each foundation model and the settlement amount S. Note that P_v includes the dead weight of the raft and the loading jig, while the settlement due to the dead weight is not included in S. In the figure, the load on the single pile is multiplied by 4 for comparison. In the piled raft, the load carried by the raft was estimated as the difference between P_v and the measured load carried by the 4 piles. For comparison, the sum of loads on the raft foundation and the 4 piles (here referred to as "simple sum") is also indicated in the figure.

Fig. 4 is a zoom-up of Fig. 3 up to S = 40 mm. While the maximum load of the piled raft showed a value close to the simple sum, the initial stiffness ($\Delta P_V/\Delta S$) was smaller than that of the simple sum. The load of the piled raft was lower than that of the simple sum up to about S = 20 mm.

3.2 Load proportion between raft and piles

Fig. 5 shows the load proportions carried the raft and the 4 piles against S. At the initial stage of loading, the load proportion carried by the piles was about 80 %. As the settlement increased, the load proportions carried by the piles decreased (the load proportions carried by the raft increased). And the load proportions carried by the raft and the piles became 50% when S reached about 20 mm. For S greater than about 150 mm, the load proportions became almost stable at the load proportions carried by the raft and the piles became about 70% and 30%, respectively.

Fig. 6 shows the axial force distribution of pile A in each load step in the piled raft. When distance from ground surface z reahed 1.5 m, the axial force decreased sharply with the increase in z. It means the pile shaft resistance is lager tuffaceous clay than that in volcanic soil layer.

Fig. 7 shows the relationship between the pile head load on each pile in the piled raft and S. For Piles B and C, the strains at the top level were not obtained successfully. Hence, the pile load was estimated from the strains measured at the second measurement level. The result of the single pile model is also shown for comparison. Although the peak load of each pile in the piled raft was comparable to that of the single pile, it is interesting to note that the peak load of each pile in the piled raft was reached at S = 10 mm, while the peak load of the single pile was mobilized at S = 5 mm.

Fig. 8 shows the relationship between the raft load in the piled raft and S. The load carried by the raft in the piled raft was calculated by subtracting the sum of the pile head load of each pile from the piled raft load P_v. The result of the raft alone model is also shown for comparison. The load carried by the raft in the piled raft was smaller than that in the raft alone for the initial stage of loading where the pile load was large. However, the load of the raft in the piled raft was almost equal to that of the raft alone model for S greater than about 20 mm.

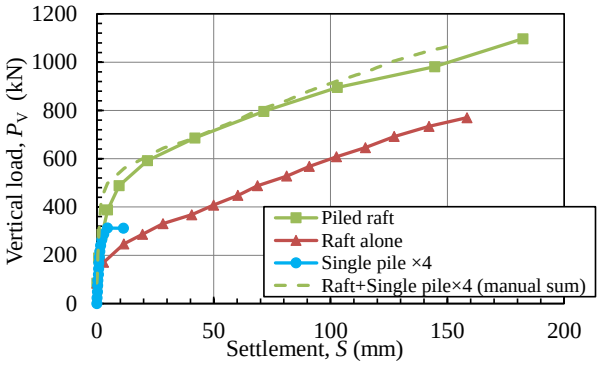

Fig. 3. *P*v-*S* relationship.

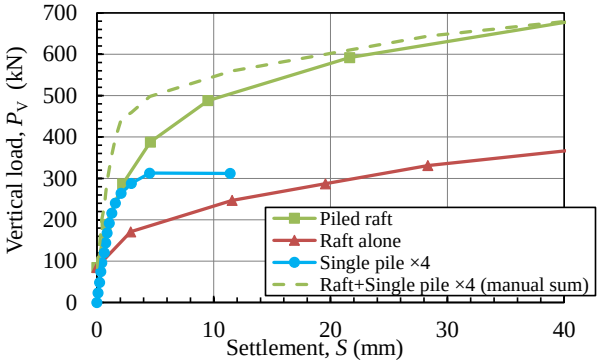

Fig. 4. *P*v-*S* relationship (magnification of initial part).

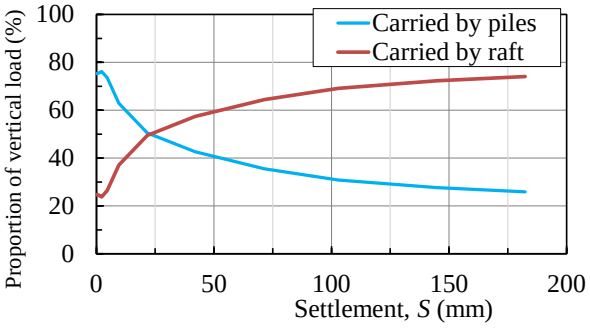

Fig. 5. Load carried between piles and raft.

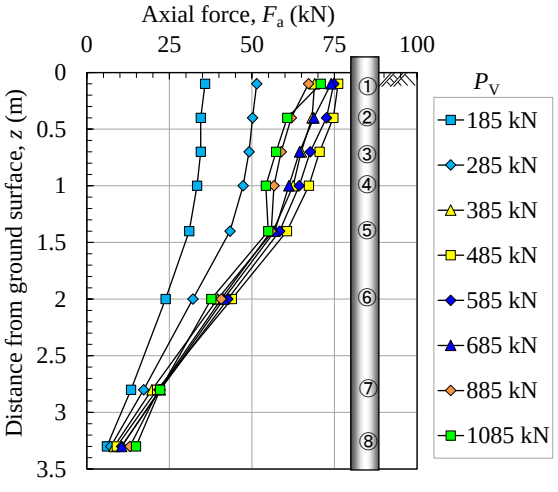

Fig. 6. Distribution of axial force (pile A).

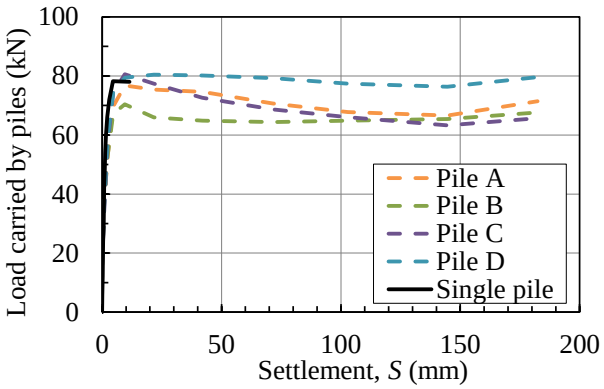

Fig. 7. Vertical load carried by piles.

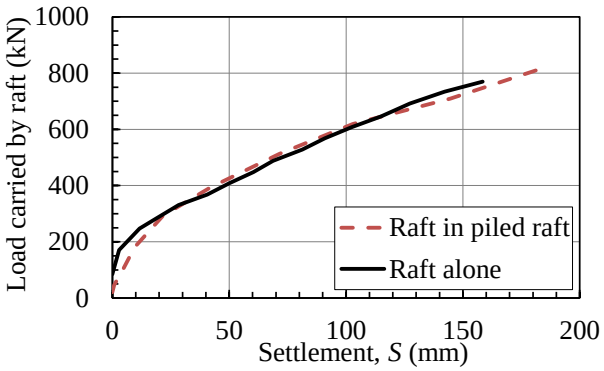

Fig. 8. Vertical load carried by the raft.

3.3 Comparison with recommendation for design of building foundations

Table 3 shows the coefficients α_R, α_P, ξ_{PR} in the piled raft in Eqs. (1) and (2), which are specified in the Recommendation for Design of Building Foundations (AIJ, 2019). The coefficients were back-calculated using the results of the experiment. Since the exact ultimate bearing capacity of the piled raft could not be confirmed in the experiment, the coefficients were calculated from the load at a settlement of 10 % of the pile diameter ($0.1D$ = 10 mm) and 10 % of the raft width ($0.1B$ = 150 mm), respectively. The settlement of the piled raft and the raft alone were calculated by adding the settlement at the initial load by the self-weight and the jig weight which was estimated from the initial stiffness ($\Delta P_V/\Delta S$) of results of each experiment. In the Recommendation, ξ_{PR} = 0.8 is recommended value, while the ξ_{PR} obtained from the experimental results was about 1.1 times the recommended value when $S = 0.1D$ and 1.4 times when $S = 0.1B$.

$$R_{PR,\,ult} = \alpha_R R_{R,\,ult} + \alpha_P R_{P,\,ult} \quad (1)$$

$$R_{PR,\,ult} = \xi_{PR}\left(R_{R,\,ult} + R_{P,\,ult}\right) \quad (2)$$

Here, $R_{PR,\,ult}$, $R_{R,\,ult}$, $R_{P,\,ult}$ are the ultimate bearing capacity of piled raft foundation, raft foundation, and pile foundation, respectively.

Table 3. Coefficients obtained from test results.

	α_R	α_P				ξ_{PR}
		Pile A	Pile B	Pile C	Pile D	
$S = 0.1D$	0.69	0.99	0.95	1.08	1.05	0.88
$S = 0.1B$	1.04	0.90	0.87	0.85	1.03	1.01

4 3D-FINITE ELEMENT ANALYSIS

4.1 Numerical model

Numerical simulations were conducted using the 3-D finite element analysis package, PLAXIS 3D. Fig. 9 shows the analytical model of the soil and the foundation model. The analytical range of soil was 20 times as large as the width of the raft model in the horizontal direction and two times as long as the length of the pile in the vertical direction. Normal displacements at the outer vertical surfaces of the ground were fixed. Vertical displacements at the bottom of the ground were fixed. Because of symmetric conditions, only a half of the foundation and the ground was modeled.

In the numerical model, the raft and the piles were simulated as elastic materials. The soils were modeled as the Mohr-Coulomb model. A fully drained condition was assumed for the ground since loading rates in the vertical load tests were very low. The piles were modeled using hybrid models of beam elements and solid elements following recommendation by Kimura and Zhang (2000). Material properties of the pile were $E = 2.06\times10^8$ kPa and $\nu = 0.3$. Interface elements of Mohr-Coulomb type were arranged along the pile shaft. The parameters of interface elements were set the same as the corresponding soil. R_{inter} was set as 1.0, assuming that the interface friction angle is equal to the internal friction angle of the surrounding soil, because of a lack of data on the interface friction angle.

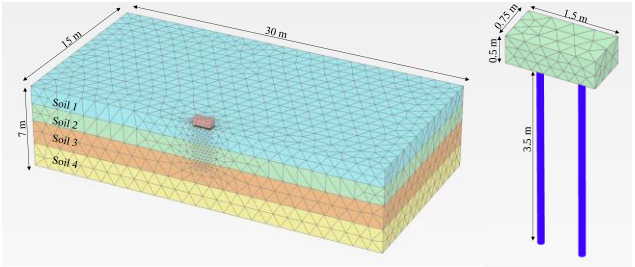

Fig. 9. Numerical model.

The soil parameters used in the analyses are listed in Table 4. In Case 1, the soil parameters were set based on the results of laboratory tests. Young's modulus E was calculated by multiplying E_{50} of the unconfined compression test by 4, according to the Specifications for Highway Bridges Part IV (JRA, 2017). c is the undrained shear strength q_u obtained from the unconfined compression test. However, since Soil 3 had a high sand content and an intermediate soil-like composition, and it was considered that the strength might have been smaller than the actual value under the stress release condition,

the converted q_u obtained from the SWS (Swedish Rotary Sounding) was adopted. Since Soil 4 is a sandy soil and unconfined compression test results were not available, E and ϕ were estimated from N value, respectively, $E = 2800N$ (kPa) and ϕ using an empirical equation proposed in Hatanaka and Uchida (1996). The parameters of interface elements were set the same as the corresponding soil.

In Case 2, the shaft resistance from the load test on the single pile was used for estimating the cohesion c of the soil. The value of E was calculated as $E = 400c$, referring according to de Sanctis and Mandolini (2006). The interface cohesion was estimated from the shaft resistance obtained from the vertical load test on the single pile with the interface friction angle of zero.

The analytical procedure was as follows.

Step 1: Self-weight analysis of the ground alone.

Step 2: Foundation wished-in-place and self-weight analysis.

Step 3: Analysis of vertical load test.

Hence, the effects of pile installation on the stress changes in the ground surrounding the piles were not explicitly considered in the analyses.

Table 4. Parameter of soil element.

Case	Soil layer	z (m)	E (kPa)	ν	c (kPa)	ϕ (°)	γ_{unsat} (kN/m^3)	γ_{sat} (kN/m^3)
1	Soil 1	-1.5	22800	0.3	43.4	0	13.6	14.6
	Soil 2	-3.0	31600	0.3	69.7	0	16.7	17.3
	Soil 3	-5.0	28400	0.3	50.0	0	16.9	18.3
	Soil 4	-7.0	16800	0.3	0	31.0	16.0	17.0
2	Soil 1	-1.5	11200	0.3	28.0	0	13.6	14.6
	Soil 2	-3.0	38400	0.3	96.0	0	16.7	17.3
	Soil 3	-5.0	28000	0.3	70.0	0	16.9	18.3
	Soil 4	-7.0	16800	0.3	0	31.0	16.0	17.0

N.B. z: Depth at bottom of the layer

4.2 Simulation results

Fig. 10 and 11 show calculated and measured results of raft alone model and single pile model, respectively. The load of the raft foundation in Case 1was much higher than the measured load (Fig. 10), while the load of the single pile in Case 1 was a little bit lower than the measured value load (Fig. 11). On the other hand, the calculated P_v - S relationship of each numerical model in Case 2 simulated the experimental results much better compared with Case 1.

Fig. 12 shows calculated and measured results of piled raft model. The P_v in Case 1 was higher than the experimental results for $S \geqq 5$ mm, while it in Case 2 showed a good agreement with the measured results.

Figure 13 shows the axial force distributions of the single pile and a pile in the piled raft at $S = 10$ mm. The calculated axial forces in Case 1 were smaller than the measured values. However, the differences of shaft resistance in differences layers can be found in the calculated axial forces in Case 2.

Figure 14 shows the load sharing ratio between the raft and the piles. In Case 1, the load sharing ratio of the pile is less than 60 % from the beginning of the loading, and the load sharing ratio of the raft is large. In Case 2, the measured load sharing ratio was well simulated.

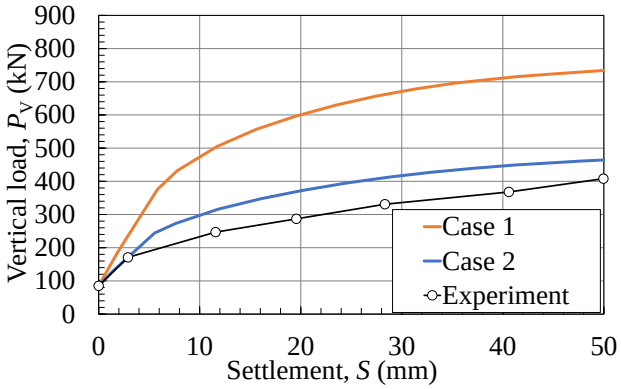

Fig. 10. Calculated and measured results of raft alone model.

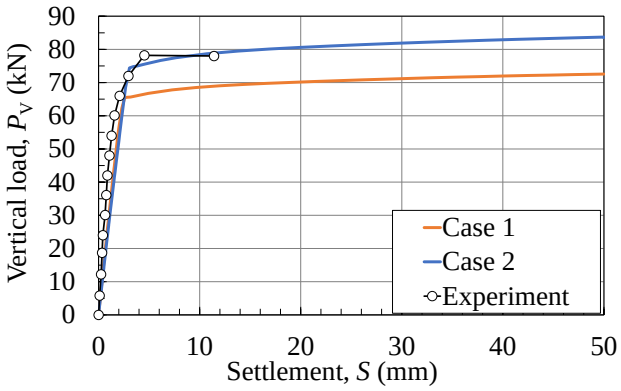

Fig. 11. Calculated and measured results of single pile model.

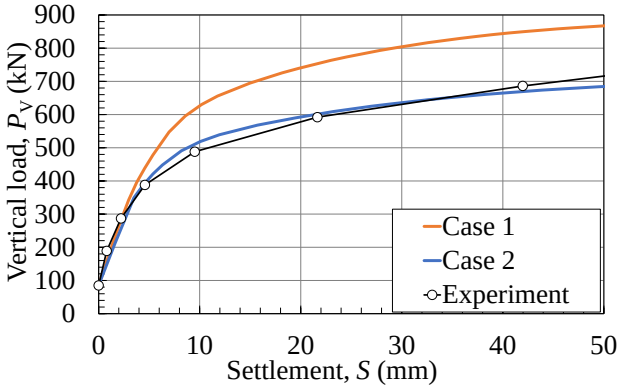

Fig. 12. Calculated and measured results of piled raft model.

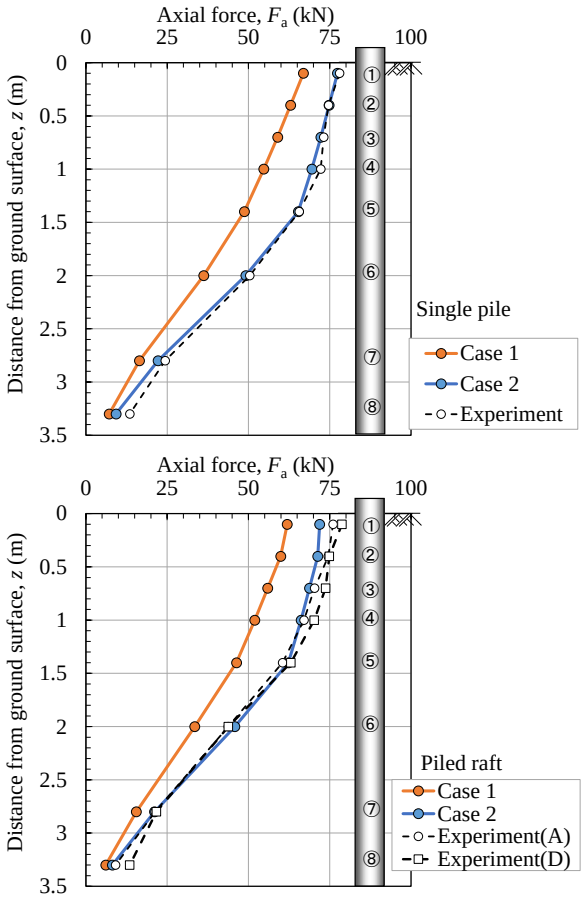

Fig. 13. Calculated and measured axial force distributions at S = 10mm (upper: Single pile, lower: Piled raft).

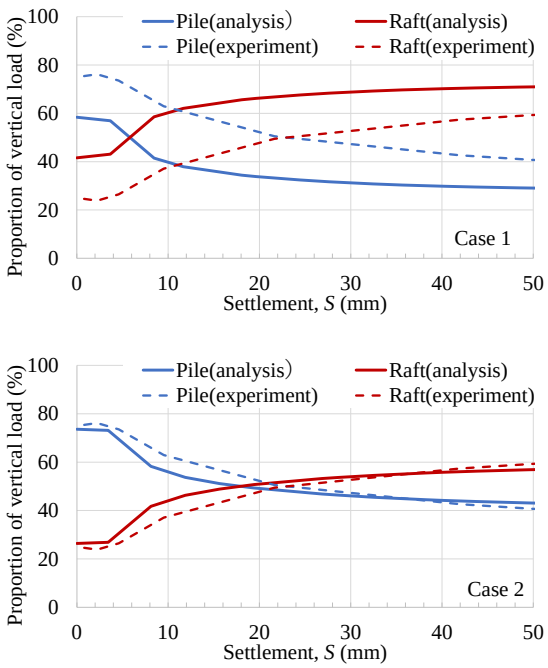

Fig. 14. Calculated and measured load sharing between raft and piles (upper: Case 1, lower: Case 2).

5 CONCLUSIONS

In this paper, the following knowledge was obtained as a result of the in-situ vertical loading test for piled raft foundation and corresponding simulations by 3D finite element analysis.

- The bearing capacity of the piled raft was almost the same as the sum of the bearing capacity of four single piles and the raft.
- The estimated bearing capacity coefficient ξ_{PR} from the experimental results was about 1.1 times at S = 0.1D and about 1.4 times at S = 0.1B, compared to ξ_{PR} = 0.8 recommended in the recommendations for the design of building foundations (AIJ, 2019).
- Two methods were used to determine the soil parameters. The parameters, estimated from the shaft resistance obtained from the vertical load test on the single pile, can describe P_v - S relationships of all foundation models well.

6 FUTURE WORK

A parametric study will be conducted in future using this numerical method under a variety of conditions incl. raft and pile dimensions in addition to re-examining the soil model.

REFERENCES

1) Architectural Institute of Japan (AIJ) (2019): Recommendation for Design of Building Foundations, ISBN978-4-8189-0652-5, Maruzen Print Co. Ltd (in Japanese).

2) de Sanctis, L. and Mandolini, A. (2006): Bearing capacity of piled rafts on soft clay soils, *Journal of Geotechnical and Geoenvironmental Engineering*, ASCE, 12, 1600-1610.

3) Hatanaka, M. and Uchida, A. (1996): Empirical correlation between penetration resistance and internal friction angle of sandy soils, *Soils and Foundation*s, 36(4), 1-9.

4) Japan Road Association (JRA) (2017): Specifications for highway bridges part IV substructure, ISBN978-4-88950-282-4, Maruzen Print Co. Ltd. (in Japanese).

5) Kimura, M. and Zhang, F. (2000): Seismic evaluation of pile foundations with three different methods based on three-dimensional elasto-plastic finite element analysis, *Soils and Foundations*, 40(5), 113-132.

6) Suzuki, N. and Hamamoto, T. (2014): Structural performance evaluation of piled-raft foundations using long-term settlement monitoring, J. Struct Constr., Eng., AIJ, 79(706), 1835-1845 (in Japanese).

7) Tsuchiya, T., Aoki, R. and Nagai, H. (2011): In-situ vertical loading tests of piled raft foundation highly organic soft ground, AIJ J. Technol. Des., 17 (36), 483-486 (in Japanese).

8) Yamashita, K., Tanikawa, T., Shigeno, Y. and Hamada, J. (2015): Numerical analysis on bearing capacity of piled raft foundations, AIJ J. Technol. Des., 21(47), 99-104 (in Japanese)